PERGAMON

Journal of Geodynamics 29 (2000) 469–499

JOURNAL OF GEODYNAMICS

Fluid involvement in normal faulting

Richard H. Sibson*

Department of Geology, University of Otago, P.O. Box 56, Dunedin, New Zealand

Abstract

Evidence of fluid interaction with normal faults comes from their varied role as flow barriers or conduits in hydrocarbon basins and as hosting structures for hydrothermal mineralisation, and from fault-rock assemblages in exhumed footwalls of steep active normal faults and metamorphic core complexes. These last suggest involvement of predominantly aqueous fluids over a broad depth range, with implications for fault shear resistance and the mechanics of normal fault reactivation. A general downwards progression in fault rock assemblages (high-level breccia-gouge (often clay-rich) → cataclasites → phyllonites → mylonite → mylonitic gneiss with the onset of greenschist phyllonites occurring near the base of the seismogenic crust) is inferred for normal fault zones developed in quartzo-feldspathic continental crust. Fluid inclusion studies in hydrothermal veining from some footwall assemblages suggest a transition from hydrostatic to suprahydrostatic fluid pressures over the depth range 3–5 km, with some evidence for near-lithostatic to hydrostatic pressure cycling towards the base of the seismogenic zone in the phyllonitic assemblages. Development of fault-fracture meshes through mixed-mode brittle failure in rock-masses with strong competence layering is promoted by low effective stress in the absence of thoroughgoing cohesionless faults that are favourably oriented for reactivation. Meshes may develop around normal faults in the near-surface under hydrostatic fluid pressures to depths determined by rock tensile strength, and at greater depths in overpressured portions of normal fault zones and at stress heterogeneities, especially dilational jogs. Overpressures localised within developing normal fault zones also determine the extent to which they may reutilise existing discontinuities (for example, low-angle thrust faults). Brittle failure mode plots demonstrate that reactivation of existing low-angle faults under vertical σ_1 trajectories is only likely if fluid overpressures are localised within the fault zone and the surrounding rock retains significant tensile strength. Migrating pore fluids interact both statically and dynamically with normal faults. Static effects include consideration of the relative permeability of the faults with respect to the country rock, and juxtaposition effects which determine whether a fault is transmissive to flow or acts as an impermeable barrier. Strong directional permeability is expected in the subhorizontal σ_2 direction parallel to

* Tel.: +64 3 479 7506; fax: +64 3 479 7527.
E-mail address: rick.sibson@stonebow.otago.ac.nz (R.H. Sibson).

PII: S0264-3707(99)00042-3

intersections between minor faults, extension fractures, and stylolites. Three dynamic mechanisms tied to the seismic stress cycle may contribute to fluid redistribution: (i) cycling of mean stress coupled to shear stress, sometimes leading to postfailure expulsion of fluid from vertical fractures; (ii) suction pump action at dilational fault jogs; and, (iii) fault-valve action when a normal fault transects a seal capping either uniformly overpressured crust or overpressures localised to the immediate vicinity of the fault zone at depth. The combination of σ_2 directional permeability with fluid redistribution from mean stress cycling may lead to hydraulic communication along strike, contributing to the protracted earthquake sequences that characterise normal fault systems.

1. Introduction

Normal fault systems are a source of seismic hazard in areas of active crustal extension, but are also structural features of economic significance. In sedimentary basins they may be key components of hydrocarbon traps, in some cases forming sealing barriers to fluid migration (Hardman and Booth, 1991) and in others, serving as cross-stratal conduits for large volume fluid flow (Burley et al., 1989). In this latter role they are critical features for hydrothermal mineralisation, being widely associated with sediment hosted Pb–Zn–Ag deposits (Goodfellow et al., 1993; Johnston et al., 1996) and in volcanic terrains hosting epithermal Au–Ag quartz vein systems (Vikre, 1989; Sillitoe, 1993). Thus, evidence for fluid interaction and involvement with normal faults at shallow crustal depths (< 1–3 km) is abundant, though explorationists are left with the problems of determining under what conditions such structures act as fluid

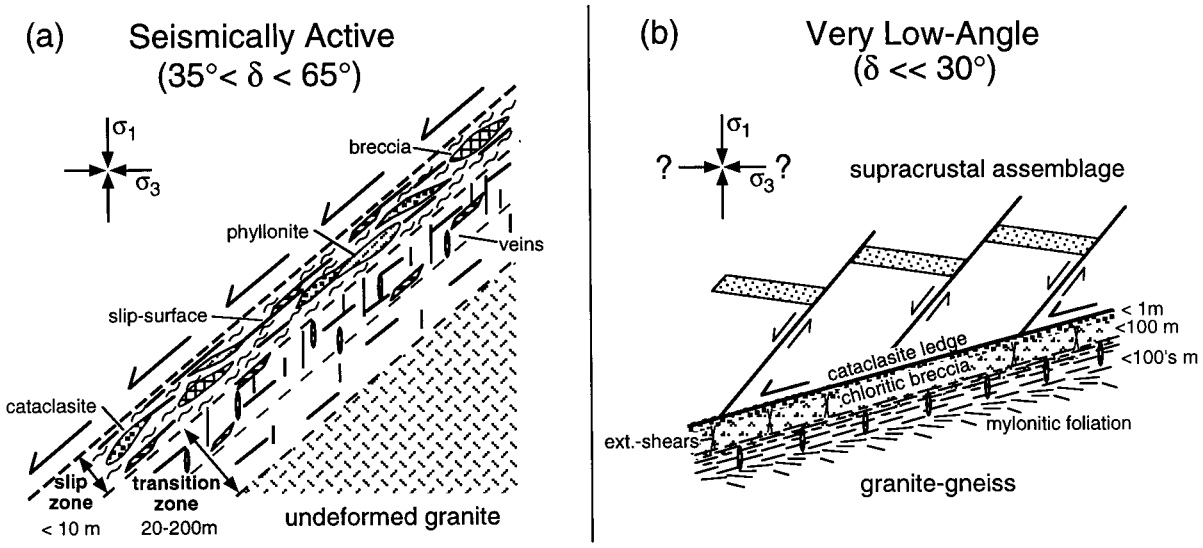

Fig. 1. Fault-rock and hydrothermal vein assemblages associated with the footwalls of: (a) the seismically active Wasatch normal fault zone, Utah (after Bruhn et al., 1994); and, (b) a metamorphic core complex (after Reynolds and Lister, 1987; Axen and Selverstone, 1994). Diagrams schematic and not to scale.

barriers or conduits, whether fault permeability is passive or dynamic, and what localises fluid flux at particular sites.

In most areas of active extensional tectonics, the seismogenic zone extends to depths of 10–15 km with larger normal fault ruptures ($M > 6$) nucleating in the lower half of the zone in well-consolidated sedimentary rocks or crystalline basement (Jackson and White, 1989). Direct evidence for fluid involvement in normal faulting at these depths is less abundant but the presence of an intergranular fluid, possibly overpressured, is of critical importance to the frictional mechanics of fault development and reactivation, reducing fault strength and potentially affecting the nucleation, arrest, and recurrence of earthquake ruptures (Sibson, 1992). Veining and hydrothermal alteration associated with fault-rock assemblages in the exhumed footwalls of steeply dipping normal faults and with metamorphic core complexes provide some information on fluid involvement with extensional fault systems at these depths and can be used to build up preliminary rheological models for the seismogenic portions of normal faults (Fig. 1).

This paper seeks not so much to provide a comprehensive review of normal fault structure and mechanics but, rather, to emphasize the importance of some of the potential fluid interactions with normal fault systems and focus attention on critical areas for future research.

2. Brittle failure modes and structural permeability in extensional regimes

Orientation of brittle structures at the time of their formation depends chiefly on the orientation of the stress field (defined by three orthogonal principal compressive stresses, $\sigma_1 > \sigma_2 > \sigma_3$) and the mode of brittle failure, but may also be affected by existing anisotropy within the rock-mass.

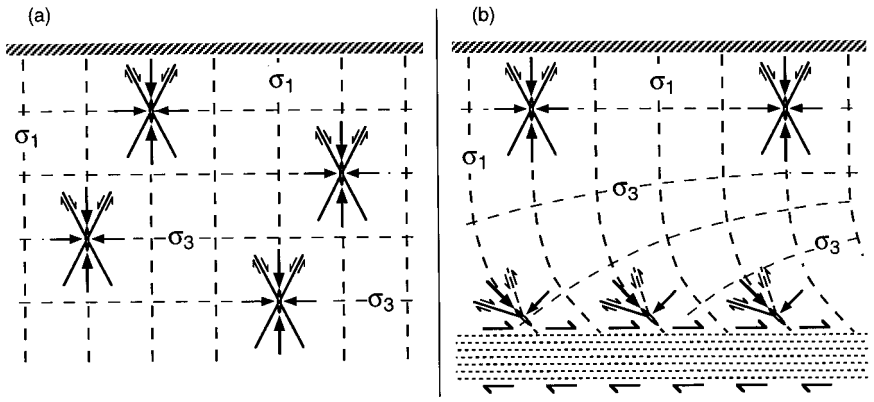

Fig. 2. Stress trajectories in extensional tectonic regimes showing expected initial orientations of brittle faults and fractures for: (a) an 'Andersonian' extensional stress state; and, (b) deflection of trajectories by basal shear stress.

2.1. Stress trajectories in extensional regimes

The simplest stress trajectory system for areas undergoing active extension is that suggested by Anderson (1905) from the boundary condition of zero shear stress imposed by the earth's free surface (taken as horizontal) with the maximum compressive stress everywhere vertical (i.e. $\sigma_v = \sigma_1$) and the least stress, σ_3, horizontal (Fig. 2). Significant departures from this stress state may occur in the near-surface as a consequence of topographic irregularities but are expected to diminish with depth. This 'Andersonian' condition is widely assumed to dominate throughout the brittle seismogenic crust.

Another boundary condition may be imposed at depth by the presence of weak ductile subhorizontal zones of decoupling in the middle to lower crust which, in their vicinity, would require stress trajectories rotated to 45° from the vertical and horizontal (Fig. 2) (Melosh, 1990; Westaway, 1998). The question is of critical importance because rotation of σ_1 trajectories to inclinations of 45° could help to explain the initiation of very low-angle brittle detachment faults (Fig. 2) that have been mapped extensively in the western United States and elsewhere (Lister and Davis, 1989). One may note, however, that sets of minor brittle structures associated with these structures are generally consistent with steep σ_1 trajectories (e.g. Reynolds and Lister, 1987; Axen and Selverstone, 1994).

Other postulated mechanisms for deviating σ_1 trajectories from the vertical at depth include stress refraction through zones of fluid overpressure (Bradshaw and Zoback, 1988) and stress reorientation in the vicinity of dykes and other intrusive bodies (Parsons and Thompson, 1993). Mechanisms for reorienting stress trajectories have been critically examined by Wills and Buck (1997), who conclude that horizontal shear stresses at depth are generally minor and

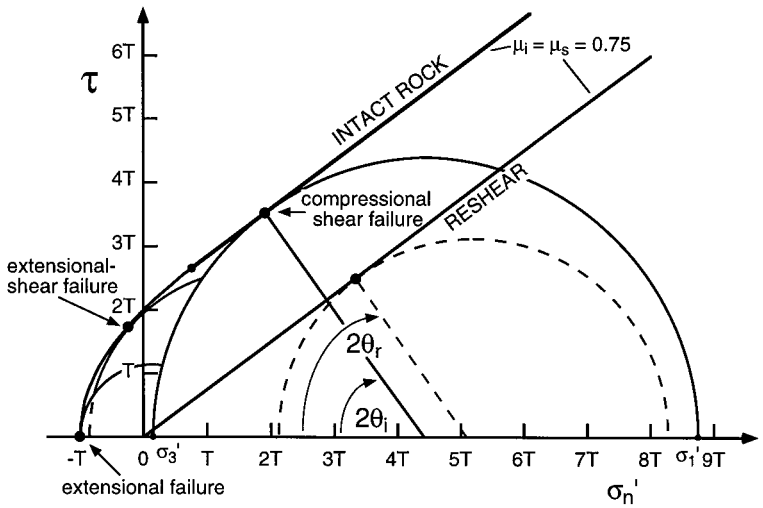

Fig. 3. Mohr diagram of shear stress, τ, against effective normal stress, σ_n' with a composite Griffith–Coulomb failure envelope for intact rock normalised to tensile strength, T, illustrating the stress conditions for the three different modes of macroscopic brittle failure, plus the reshear condition for an existing cohesionless fault ($\mu_i = \mu_s = 0.75$).

Table 1
Criteria for brittle failure and reshear ($\mu_i = \mu_s = 0.75$)

Failure mode (field of application)	τ/σ_n' space P_f dependence	Orientation with respect to stress field ($\sigma_v = \sigma_1$)
Extensional (Griffith criterion)	$\tau^2 = 4T(\sigma_n - P_f) + 4T^2$	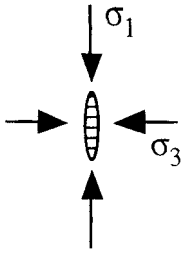
$(\sigma_1 - \sigma_3) < 4T$	$P_f = \sigma_3 + T$	
Extensional-shear (Griffith criterion)	$\tau^2 = 4T(\sigma_n - P_f) + 4T^2$	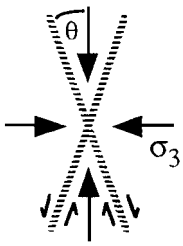
$4T < (\sigma_1 - \sigma_3) < 5.66T$	$P_f = \sigma_3 + \frac{[8T(\sigma_1 - \sigma_3) - (\sigma_1 - \sigma_3)^2]}{16T}$	
Compressional-shear (Coulomb criterion)	$\tau = C + \mu_i(\sigma_n - P_f)$	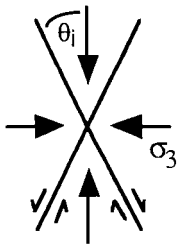
$(\sigma_1 - \sigma_3) > 5.66T$	$P_f = \sigma_3 + \frac{[8T - (\sigma_1 - \sigma_3)]}{3}$ for $\mu_i = 0.75$	
Reshear of cohesionless fault (Amontons law)	$\tau = \mu_s(\sigma_n - P_f)$	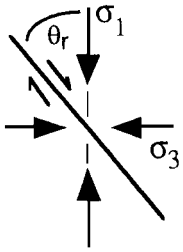
	$P_f = \sigma_3 - \frac{(\sigma_1 - \sigma_3)(1 - 0.75 \tan\theta_r)}{0.75(\cot\theta_r + \tan\theta_r)}$ for $\mu_s = 0.75$	

insufficient to deviate σ_1 trajectories significantly from the vertical through most of the seismogenic crust.

2.2. Brittle failure modes

Three modes of macroscopic brittle failure (shear fractures (faults), pure extension fractures, and hybrid extensional-shear fractures) may occur in intact rock with predictable orientations to the principal stress axes (Fig. 3). The type of failure that occurs is highly sensitive to the level of fluid-pressure, P_f, in a fluid-saturated rock-mass where effective principal compressive stresses (Hubbert and Rubey, 1959) are:

$$\sigma_1' = (\sigma_1 - P_f) > \sigma_2' = (\sigma_2 - P_f) > \sigma_3' = (\sigma_3 - P_f) \tag{1}$$

At a depth, z, the level of fluid-pressure may be defined in terms of the pore-fluid factor:

$$\lambda_v = \frac{P_f}{\sigma_v} = fr\frac{P_f}{\rho gz} \tag{2}$$

where ρ is the average rock density and g is gravitational acceleration, so that the effective vertical stress is

$$\sigma_v' = (\sigma_v - P_f) = \rho gz(1 - \lambda_v) \tag{3}$$

A hydrostatic fluid pressure state ($\lambda_v \sim 0.4$) obtains when pore and/or fracture space is interconnected up to the water table (assumed at the earth's surface); suprahydrostatic fluid pressures are represented by $0.4 < \lambda_v < 1.0$, and lithostatic pressures by $\lambda_v = 1.0$.

Stress/fluid-pressure conditions under which the different failure modes develop are illustrated on a standard Mohr diagram of shear stress, τ, plotted against effective normal stress, $\sigma_n' = (\sigma_n - P_f)$ with a composite Griffith–Coulomb failure envelope for intact, homogeneous and isotropic rock normalised to tensile strength, T (after Secor, 1965) (Fig. 3). The reshear condition for a cohesionless existing fault (equivalent to the failure condition for a cohesionless aggregate) is also illustrated. For simplicity, the slopes of the linear portions of the intact failure envelope in the compressional field and the reshear criterion for a cohesionless existing fault are both constructed with slopes of 0.75, corresponding to the average of the experimentally determined range for internal friction ($0.5 < \mu_i < 1.0$) (Jaeger and Cook, 1979) and near the middle of (Byerlee's, 1978) range for sliding friction ($0.6 < \mu_s < 0.85$) (see Sibson, 1998). The different failure criteria are listed in Table 1 in both their standard forms in τ/σ_n' space and, to emphasise their dependence, as functions of fluid-pressure level. For a particular rock-type, the different modes of failure may be induced either by changing the differential stress state, or by increasing fluid-pressure with differential stress held fixed.

Within a particular rock-unit, the failure mode depends on the balance between the differential stress, $(\sigma_1 - \sigma_3)$, and rock tensile strength, T (Secor, 1965). When $(\sigma_1 - \sigma_3) < 4T$, extension fractures form in accordance with the hydraulic fracture criterion along planes perpendicular to the least compressive stress. When $(\sigma_1 - \sigma_3) > 5.66T$, shear fractures (faults) form in accordance with the Coulomb criterion along planes containing the σ_2 axis at angles,

$\theta_i = 27^\circ \pm 5^\circ$ to σ_1 (allowing for the $0.5 < \mu_i < 1.0$ experimental range). Note that Coulomb shear discontinuities may also develop at similar orientations in cohesionless aggregates. When $4T < (\sigma_1 - \sigma_3) < 5.66T$, extensional-shear fractures form along planes also containing the σ_2 axis but at lower angles ($\theta < \theta_i$) to σ_1. Reshear of existing cohesionless faults (here restricted to existing faults containing the σ_2 axis) is a function of their orientation as well as differential stress and fluid-pressure levels.

Thus for the standard 'Andersonian' extensional stress state ($\sigma_v = \sigma_1$), extension fractures should be vertical, normal faults should dip at angles of 58°–68°, and extensional-shears should have still steeper inclinations (Fig. 2).

2.3. Extensional failure mode plot

The P_f-dependent forms of the failure criteria listed in Table 1 may be used to define brittle failure conditions on plots of differential stress against effective vertical stress, σ_v', which can then be converted to equivalent depths for particular values of the pore-fluid factor, λ_v (Sibson,

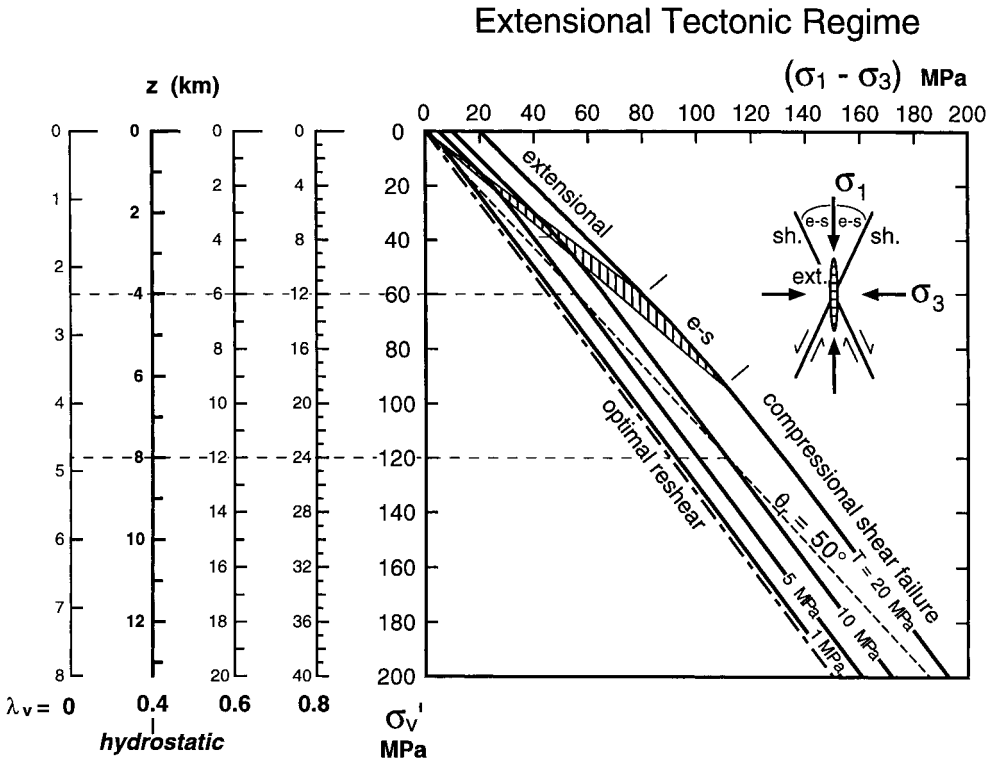

Fig. 4. Brittle failure mode plot of differential stress ($\sigma_1 - \sigma_3$) versus effective vertical stress, σ_v' in an extensional regime with $\sigma_v = \sigma_1$. Effective vertical stress can be equated to depth for different values of the pore-fluid factor, λ_v. Failure curves are plotted for intact rock with $T = 1,5,10$, and 20 MPa and the reshear of both an optimally oriented cohesionless normal fault, and one dipping at 40° ($\mu_i = \mu_s = 0.75$). Different failure mode fields are outlined.

1998). For an 'Andersonian' extensional regime ($\sigma_v = \sigma_1$), failure curves are constructed for intact rocks of various tensile strength, T, a measure of rock 'competence' (Fig. 4). Intact tensile strength varies from typical values of 1–10 MPa for most sedimentary rocks to 20 MPa or more for crystalline rocks (Lockner, 1995). Each failure curve defines transitions from purely extensional fracturing in the near-surface, through extensional-shear, to compressional shear failure with increasing σ_v, the equivalent depths for the transitions increasing with rock tensile strength. For example, under hydrostatic fluid pressures ($\lambda_v \sim 0.4$), pure extension fracturing for $T = 10$ MPa extends to depths of ~2 km and the transition from extensional-shear to compressional-shear failure occurs at depths of ~3 km. Processes such as hydrothermal silicification, by increasing tensile strength of the rock mass, may thereby increase the depth to which extension fracturing may occur.

Note that at high values of σ_v' brittle structures can only form by compressional shear failure, but when σ_v' is low the mode of brittle failure becomes extremely sensitive to variations in rock 'competence' reflecting tensile strength. Mixed mode failure is then likely in a heterogeneous rock-mass. Another important point, apparent from both Figs. 3 and 4, is that the presence of an existing throughgoing cohesionless fault that is favourably oriented for frictional reactivation prevents attainment of the tensile overpressure condition ($P_f > \sigma_3$) needed for hydraulic extension fracturing and extensional-shear failure. Formation of extension fractures and extensional-shears is therefore only to be expected: (i) in intact crust; (ii) when existing faults have become severely misoriented for frictional reactivation (Sibson, 1985a); or,

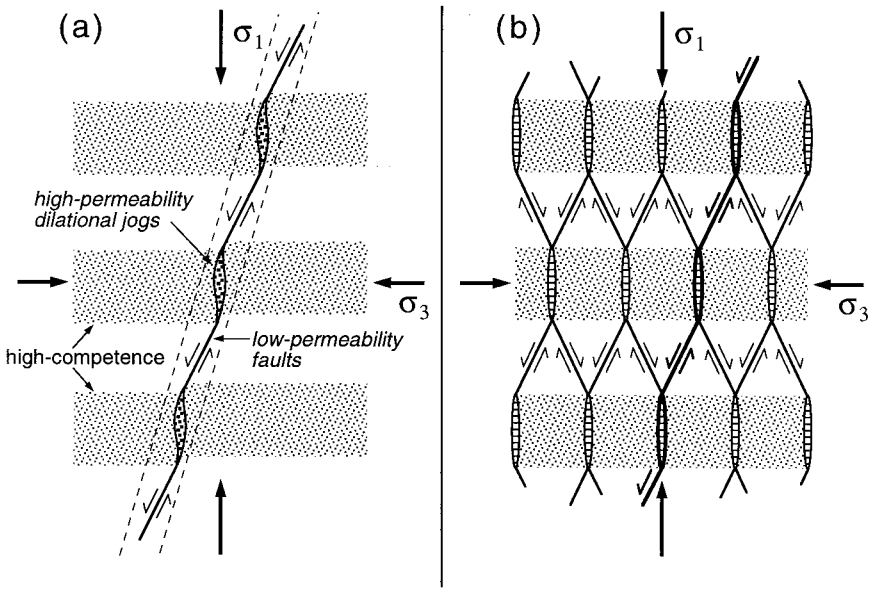

Fig. 5. Influence of competence (tensile strength) layering on brittle failure mode in an extensional regime: (a) composite normal fault refracting through high-competence layers to form dilational jogs; (b) development of an extensional fault-fracture mesh with extension veins forming in the more competent layers (incipient amalgamation of components into a throughgoing fault is represented by the bolder lines).

(iii) when existing faults have regained cohesive strength through hydrothermal cementation, etc.

2.4. Composite normal faults and fault-fracture meshes

At low σ_v', the sensitivity of brittle failure mode to varying tensile strength causes refraction of low-displacement normal faults as they transect layers of varying competence, resulting in a composite structure of en échelon Coulomb shears linked by dilational jogs comprising one or more extensional or extensional-shear fractures in the more competent layers (Fig. 5). In similar circumstances, fluid infiltration through a heterogeneous rock-mass undergoing extension may lead to development of a fault-fracture mesh made up of Coulomb shears (faults), extensional-shears, and extension fractures interlinked throughout a substantial rock volume (Hill, 1977; Sibson, 1996). Mesh structure will in general be rather irregular unless the stress field is symmetric with respect to competence layering (Fig. 5(b)).

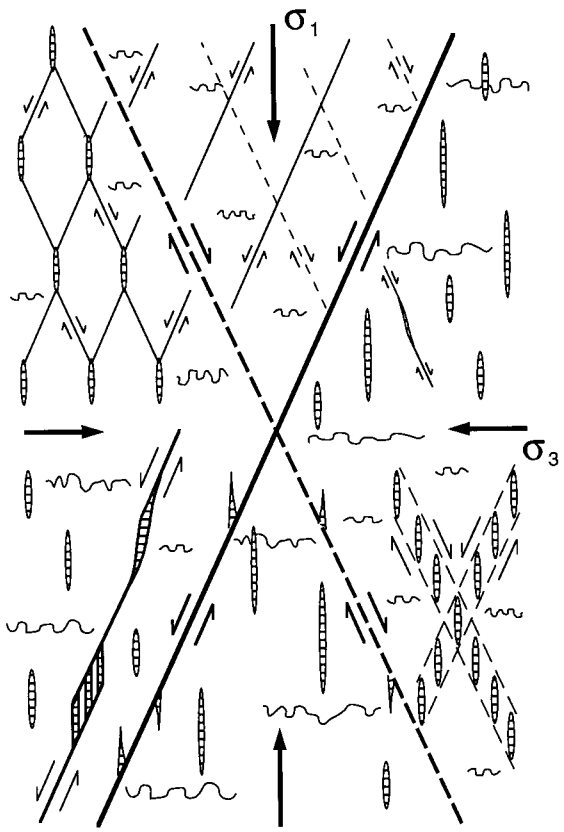

Fig. 6. Stress-controlled components of structural permeability in various combinations within an extensional stress field with $\sigma_v = \sigma_1$ (shear-sense indicators define faults (Coulomb shears); extension fractures and extensional-shears (cross-hatched); stylolites (squiggly lines)). Note common intersection of all stress-controlled components in the σ_2 direction.

Activation of meshes comprising interlinked shear and extensional fractures again requires the tensile overpressure condition ($P_f > \sigma_3$ or $\sigma_3' < 0$) to be met, at least locally, and can generally occur only in the absence of a throughgoing normal fault that is favourably oriented for reactivation in the circumstances defined above. Progressive interlinkage of mesh components may in fact eventually lead to the development of a throughgoing fault (Fig. 5(b)), preventing further attainment of the tensile overpressure condition and continued mesh activation. In many cases mesh development therefore appears to be a precursor to the development of throughgoing normal faults. Fault-fracture meshes are especially likely to develop in the near-surface where they may form under hydrostatic fluid pressure conditions, but they may also develop at depth in regions of suprahydrostatic overpressuring, or where σ_3 has been locally reduced as a consequence of stress heterogeneity within dilational jogs, etc. (Segall and Pollard, 1980). Fluid activation of fault-fracture meshes provides a plausible volumetric source for earthquake swarm activity distributed throughout a substantial rock volume (Hill, 1977).

2.5. Components of structural permeability

Stress-controlled structures affecting rock permeability include brittle faults, microcracks, extensional and extensional-shear fractures, and stylolitic solution seams. Their orientations with respect to an extensional stress state are illustrated in Fig. 6, along with some of the interlinkages that are observed. Different combinations of these features may contribute to the bulk permeability of the rock mass but the permeability of individual components is not simply predictable and may also be time-dependent through processes such as hydrothermal cementation (Sibson, 1994). This is especially the case for faults where fault permeability

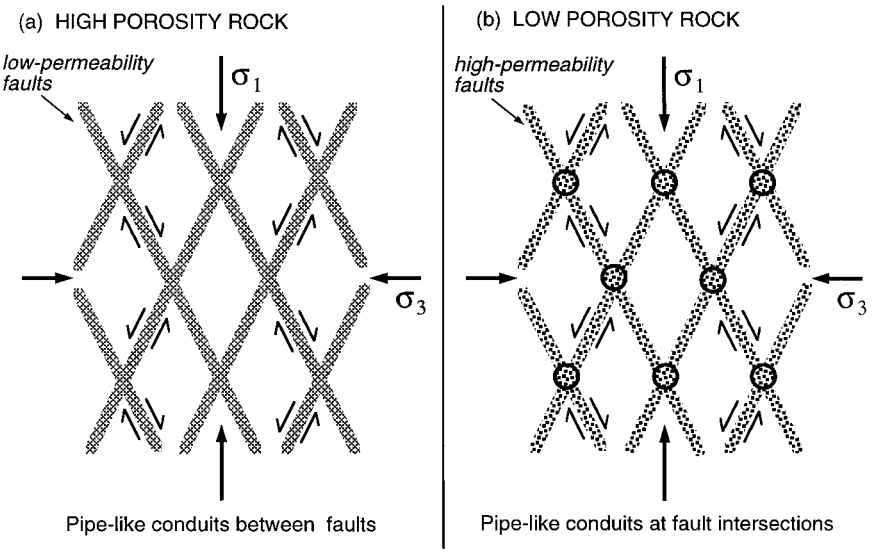

Fig. 7. Conjugate sets of normal faults imposing σ_2 directional permeability: (a) low-permeability faults in high-porosity rocks; (b) high-permeability faults in low-porosity rocks.

relative to the country rock depends critically on the nature of that rock and may also vary with displacement, gouge development, and hydrothermal cementation. As a general rule, minor faults developed in strong, initially low-porosity rocks enhance local permeability through the mismatch of opposing walls and through cataclastic brecciation (Brown and Bruhn, 1996). Interestingly, borehole measurements in areas of fractured crystalline bedrock show that it is generally the fractures that are most favourably oriented for shear reactivation in the prevailing stress field that are most hydraulically conductive (Barton et al., 1995; Hickman et al., 1997). In contrast, faults developing in initially high porosity sedimentary or volcanic rock, may through grain comminution, porosity collapse and alteration to clay-rich

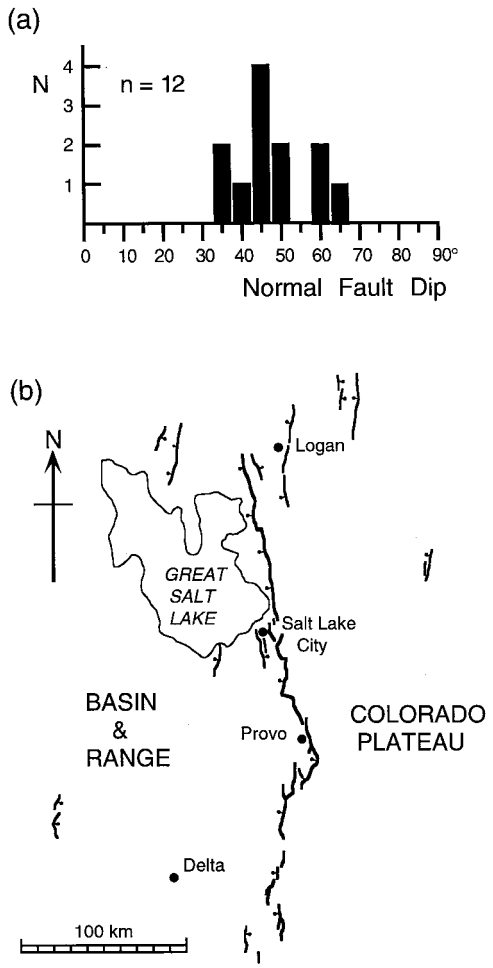

Fig. 8. (a) Global dip histogram for $M > 5.5$ normal fault ruptures with slip vectors raking within $\pm 30^\circ$ of dip direction (data from complication by Jackson and White, 1989). Histogram drawn with 5° bins centred on 30°, 35°, etc. because of the tendency to 'round' dip estimates to the nearest 5°. Note that individual dip estimates are uncertain by at least $\pm 5^\circ$. (b) Young (< 15 ka) active normal faults in the vicinity of the Wasatch Front, Utah (after Machette et al., 1991).

assemblages, form 'deformation bands' that are relatively impermeable with respect to the wall-rock (Antonellini and Aydin, 1994). Both macroscopic and microscopic extensional fracturing enhance permeability in the σ_1/σ_2 plane provided the cracks remain uncemented, the effect becoming more pronounced as $P_f \rightarrow \sigma_3$, with open gapes when $P_f > \sigma_3$. Under these conditions, extensional-shears likewise form gaping conduits for large volume flow. Stylolitic seams orthogonal to σ_1 restrict flow perpendicular to the σ_2/σ_3 plane (Groshong, 1988).

Note that the common intersection of these stress-controlled features lies parallel to the σ_2 axis. Various combinations of these stress-controlled permeability components such as dilational fault jogs, conjugate tension gash shear zones, and Hill (1977) fault-fracture meshes may therefore lead to strong directional permeability in that direction provided there is adequate 3D continuity and interconnection between the various components. Fig. 7 illustrates how σ_2 directional permeability may develop from conjugate normal fault sets regardless of whether the faults are low-permeability structures in rocks of high porosity and intrinsic permeability, or comparatively high-permeability structures disrupting low-porosity rocks.

3. Architecture of major seismogenic normal fault systems

In recent years there has been considerable controversy over the geometry of normal fault systems, partly because of contradictory information from disparate sources (Jackson and White, 1989). Seismic reflection profiling and drilling within the top few kilometres of sometimes undercompacted sedimentary basins have demonstrated the existence of listric normal faults that flatten with depth into detachment horizons (Bally et al., 1981). Many of these structures seem to be 'growth' faults that evolved during sedimentation and progressive compaction within the basins (see Vendeville, 1991). Extensional 'detachment' faults that were apparently active at very low dips have also been described in association with metamorphic core complexes, often juxtaposing consolidated and faulted sedimentary and/or volcanic assemblages in their hanging wall against crystalline rocks in their footwalls (e.g. Lister and Davis, 1989; John and Foster, 1993).

In contrast, seismogenic normal faults with down-dip rupture dimensions of the order of 10 km, generally rooted in crystalline basement, appear as predominantly planar features in section and are often part of rotating 'domino' sets (Jackson and White, 1989; Westaway, 1991). Dips of these active normal faults determined seismologically from $M > 5.5$ earthquakes range from 35°–65° (Fig. 8(a); note that this histogram is based on the data set of Jackson and White (1989) restricted to ruptures where the fault plane has been positively discriminated and the slip vector rakes within $\pm 30^\circ$ of the dip direction). This observed dip range is entirely consistent with normal faults initiating with steep 'Andersonian' dips, then domino rotating down to frictional lock-up at dips predictable from Byerlee friction values and vertical σ_1 trajectories (Sibson, 1985a; see Section 4.5). This discussion focuses principally on large planar seismogenic faults capable of giving rise to moderate to large earthquakes ($5.5 < M < 7.5$), but some of the concepts developed are also relevant to normal faulting at shallow depths in sedimentary basins.

3.1. Along-strike segmentation

Large seismically active normal fault systems typically exhibit somewhat scalloped fault traces, often concave in the dip direction, and are segmented along strike, as along the Wasatch Front at the eastern margin of the Great Basin in Utah (Fig. 8). Individual segments typically extend for 10–30 km along strike (Machette et al., 1991), distances that are 1–2 times the usual thickness of the seismogenic crust in areas of rifting, though longer segments are known, for instance in the East African Rift system where the seismogenic zone is also notably deeper (Jackson and Blenkinsop, 1997). Segments are linked through relay ramps which may be 'soft', involving warping and diffuse deformation, or through 'hard' linkage in the form of clear-cut transfer faults (Peacock and Sanderson, 1991; McClay and Khalil, 1998; Walsh and Watterson, 1991). These relay zones are sites of stress heterogeneity and can be viewed as the process zones associated with the growth of individual segments and their eventual linkage. The processes by which small normal faults developed within extending crust amalgamate and grow into larger scale system is an area of active current research (e.g. Cowie, 1998).

3.2. Scaling relationships

Large normal fault ruptures occupying the full depth of the seismogenic zone generally involve one or more segment lengths within these systems. For individual ruptures, the ratio of maximum incremental displacement, D_{mi}, to rupture length, L, typically lies in the range $10^{-5} < D_{mi}/L < 10^{-4}$, and can be fitted approximately by

$$D_{mi} = 10^{-5} L^{1.5} \tag{4}$$

an empirical relationship derived from the extensive data base compiled on fault surface breaks by Wells and Coppersmith (1994). This may be contrasted with the scaling relationships for finite maximum displacement, D_{mf}, and finite fault length, L_f, where $10^{-3} < D_{mf}/L < 10^{-1}$ (Scholz et al., 1993; Schlische et al., 1996). In a data set dominated by normal faults, Schlische et al. (1996) obtain:

$$D_{mf} \sim 0.03 L^{1.06} \tag{5}$$

as a best-fit scaling relationship. A typical 20 km long normal fault segment would therefore, be expected to have a maximum throw of $\backsim$1 km.

4. Deep structure and frictional mechanics of crustal-scale normal faults

Fault-rock assemblages on the exhumed footwalls of major normal faults and metamorphic core complexes provide information on deformation processes and physical conditions at depth and can be used to build simple models of normal fault rheology throughout and beneath the seismogenic zone.

4.1. Fault rock distribution with depth

Stewart and Hancock (1991) have described normal fault footwall assemblages in competent rocks (e.g. Mesozoic platform carbonates of the Aegean) that have been exhumed from depths of up to perhaps a kilometre or so. These assemblages comprise well defined principal slip surfaces with strong frictional wear striations, grooving, and other slip-plane phenomena which directly overlie tabular zones of cohesive breccia–microbreccia, in turn overlying zones of incohesive carbonate breccia and extensive shatter belts in the very near-surface that at depth become variably cemented stylo-breccias. Gouge, breccia, and cataclasite are also the dominant fault-rocks preserved in the footwalls of most normal faults developed in quartzo-feldspathic crust, for example the granitoid-derived fault-rock assemblages described from the footwalls of major normal faults in the Great Basin of the Western United States (Parry and Bruhn, 1987; Power and Tullis, 1989; Bruhn et al., 1994; Seront et al., 1998).

In the footwall of the major Wasatch Fault in Utah (Figs. 1(a) and 8(b)), essentially undeformed quartz-monzonite with a low fracture density and comparatively minor hydrothermal alteration passes upwards into a transition zone, tens to hundreds of metres in thickness, of variably fractured and altered rock. This in turn gives way to an intensely deformed and hydrothermally altered 'slip zone' with a preserved thickness of ~10 m comprising discontinuous lenses of breccia, finely comminuted cataclasite, and highly altered and partially recrystallised phyllonite, all penetrated by large striated and grooved slip surfaces (Bruhn et al., 1994). Analyses of CO_2-rich fluid inclusions within an epidote–chlorite–sericite–magnetite alteration assemblage associated with the phyllonites suggest that the assemblage has

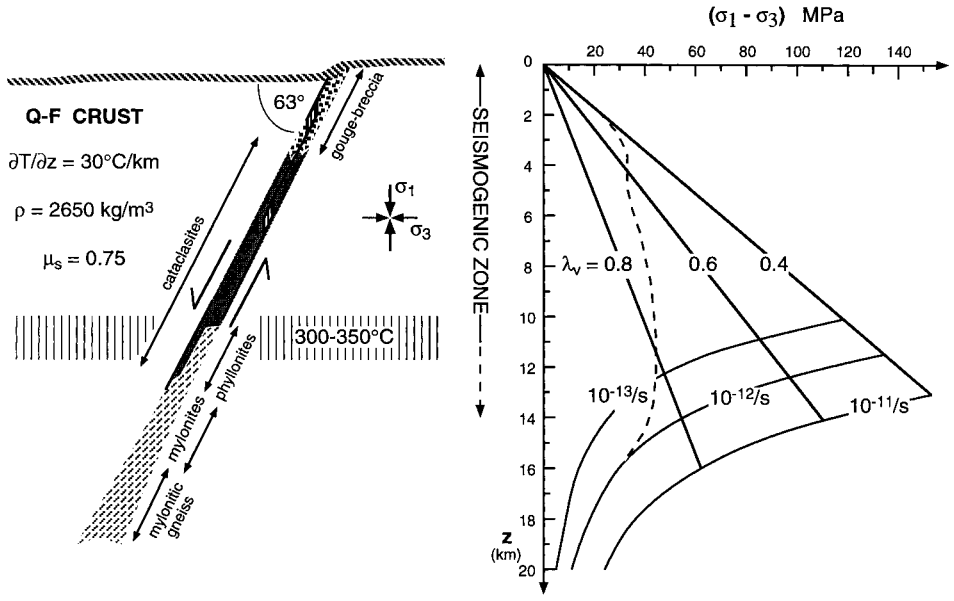

Fig. 9. Fault rock distribution and rheological strength profile for an optimally oriented crustal-scale normal fault ($\mu_s = 0.75$; $\rho = 2650$ kg/m^3; wet quartzite flow law from Paterson and Luan (1990); $\partial T/\partial z = 30$°C/km; varying λ_v).

been exhumed from depths of at least 11 km (Parry and Bruhn, 1986, 1987). Moreover, the analyses demonstrate that fluid pressures in the fault rock assemblages were fluctuating between near-lithostatic and near-hydrostatic levels. Similar evidence for fluid pressure cycling has also been obtained from the footwall of the Dixie Valley fault zone in Nevada (Parry and Bruhn, 1990).

Footwalls of metamorphic core complexes (Fig. 1(b)) are generally made up of a tabular deformation zone, tens to hundreds of metres thick, of quartzo-feldspathic mylonites and mylonitic gneisses developed under greenschist to amphibolite facies metamorphic conditions which, towards their top, are overprinted by brittle cataclastic deformation (breccias to cataclasites) with intense chloritic alteration and capped by a sharply defined cataclasite ledge (Davis, 1983; Lister and Davis, 1989). These footwall assemblages demonstrate that shearing deformation in extensional fault systems, in at least some circumstances, remains well localised through the middle and lower crust.

A general downwards progression in dominant fault-rocks:

$$\text{gouge} - \text{breccia} \rightarrow \text{cataclasite} \rightarrow \text{phyllonite} \rightarrow \text{mylonite} \rightarrow \text{mylonitic gneiss}$$

is therefore inferred for a normal fault zone developed in quartzo-feldspathic crust (Fig. 9). In most cases, estimates for the transition depths between different fault-rock types are little more than guesses. However, the transition from pressure-sensitive cataclastic deformation associated with unstable frictional sliding at high crustal levels to well-ordered penetrative fabrics in mylonitic rocks is generally inferred to represent the transition from seismic to aseismic shearing with depth, though it is increasingly recognised that the base of the seismogenic zone is transitional with a complex mixture of seismic and aseismic shearing processes, perhaps accompanied by fluid-pressure cycling (Sibson, 1983, 1994). Phyllonite development with hydrothermal reaction softening of feldspar as well as some crystal plastic deformation of quartz (Evans, 1990) takes on special importance because of its likely correlation to the transition between cataclastic and crystal plastic rheologies around the base of the seismogenic zone. The estimated 11 km (350°C) depth for the cataclasite–phyllonite transition on the Wasatch fault, coupled with the evidence for fluid-pressure cycling (Parry and Bruhn, 1986) is thus of special significance.

4.2. Permeability structure and fluid pressure regimes

For the 'Andersonian' extensional stress state ($\sigma_v = \sigma_1$), both steep normal faults and subvertical extension fractures generally cut steeply across strata, providing potential drainage paths for any fluid overpressures that may develop at depth. This raises the issue as to the level of fluid overpressuring that can be sustained in extensional tectonic regimes. Overpressuring is, however, widely reported from beneath thick shale sequences in extensional basins where active growth faulting is occurring, along with evidence from thermal plumes in the overlying portions of the basins for episodic bleed-offs from the overpressured zones (Roberts et al., 1996; McKenna and Sharp, 1997). A critical question, therefore, is whether the permeability structure in seismically active normal fault zones developed within competent basement rocks allows significant overpressures to develop and be maintained at depth.

General models developed for the permeability structure of large normal fault zones (Fig. 1)

suggest that a relatively impermeable fault core of fine-grained cataclasite–ultracataclasite or phyllonite is flanked by a damage zone of fractured rock that maintains comparatively high, though anisotropic, permeability relative to both the protolith and the core zone (Caine et al., 1996). Permeabilities estimated by modelling from measured fractured sets and from direct laboratory measurements of cored samples under a range of effective confining pressures vary from 10^{-13} to 10^{-20} m^2 with the higher permeabilities generally associated with the damage zone (Bruhn et al., 1994; Evans et al., 1997; Seront et al., 1998). These permeability estimates are substantially greater than the permeabilities of $<10^{-20}$ m^2 generally cited as necessary to maintain fluid overpressures at depth (Brace, 1984). One may question, however, whether material sampled in the near-surface after undergoing exhumation, relief of confining pressure, and weathering can ever be adequately representative of the permeability structure at seismogenic depths, even after reimposition of confining pressure. For instance, Morrow and Lockner (1997) demonstrate that granite core recovered from deep boreholes yields permeabilities that are several decades lower than equivalent weathered surface granites. Moreover, recent experimental work has shown how hydrothermal flow and precipitation may dramatically reduce existing granite permeability over short time periods (Moore et al., 1994).

In addition, geological evidence for fluid flux and overpressuring localised within normal fault zones at seismogenic depths is widespread. Fluid inclusion studies from exhumed normal fault footwalls indicate cycling of fluid pressure from near-lithostatic to hydrostatic values (Parry and Bruhn, 1986, 1990). Within metamorphic core complexes, extensive hydration and retrogression within the footwall chloritic breccias indicate large fluid flux (Kerrich, 1988) and there is evidence that the tensile overpressure condition, $P_f > \sigma_3$, was met at least locally from the existence of arrays of steep extension veins in the mylonitic footwalls (Reynolds and Lister, 1987) and the widespread occurrence of sets of conjugate normal-sense extensional-shears intersecting at low angles within the chloritic breccias (Axen and Selverstone, 1994). Thus there is accumulating evidence that deep portions of normal fault zones in crystalline crust are significantly overpressured with respect to their surroundings.

4.3. Rheological strength profile for an optimally oriented crustal-scale normal fault

A rheological strength profile of differential stress against depth, z, has been constructed for an optimally oriented normal fault developed in quartzo-feldspathic crust with a geothermal gradient of 30°C/km and average density $\rho = 2650$ kg/m^3 using the standard procedure of Sibson (1983). Frictional strength in the uppermost crust is taken to be governed by 'Byerlee' friction ($\mu_s = 0.75$) under different fluid pressure regimes ($\lambda_v = 0.4$ (hydrostatic), 0.6, and 0.8). For a cohesionless normal fault containing the σ_2 axis at an angle, θ_r to a vertical σ_1 direction, the 2D reshear criterion (Table 1) may be rewritten as

$$(\sigma_1 - \sigma_3) = \frac{\mu_s(\tan\theta_r + \cot\theta_r)}{(1 + \mu_s\cot\theta_r)}\rho g z(1 - \lambda_v) \tag{6}$$

which reduces to

$$(\sigma_1 - \sigma_3) = 0.75\rho g z(1 - \lambda_v) \tag{7}$$

for the special situation where the fault is optimally oriented for frictional reactivation at $\theta_r = 0.5\tan^{-1}(1/\mu_s) \sim 27^\circ$ when $\mu_s = 0.75$, corresponding to a fault dip of 63° (Fig. 9).

Flow strength of the localised ductile shear zone in the quasi-plastic regime is assumed to be governed by the 'representative' quartzite flow law of Paterson and Luan (1990), under shear strain-rates in the range 10^{-13}–10^{-11}/s, corresponding to time-averaged slip-rates of 0.1–1 mm/yr across tabular shear zones ranging in width from approximately 30 to 3 m. Given the uncertainties in extrapolating laboratory flow laws to the natural environment (Rutter and Brodie, 1992), and the likelihood of additional flow and weakening mechanisms (e.g. solution transfer, reaction softening, fluid overpressures) operating, especially in the region around the base of the seismogenic zone (Evans, 1990), all that can really be said is that this hydrostatic strength profile likely provides an upper bound to the strength of optimally oriented normal faults in quartz-rich crust. A more 'realistic' strength profile in a fault zone that becomes progressively overpressured with depth is illustrated by the dashed line in Fig. 9.

4.4. Load-weakening character

During loading of a normal fault to failure by progressive crustal extension, horizontal stress ($\sigma_h = \sigma_3$) decreases while vertical stress ($\sigma_v = \sigma_1$) stays constant (Fig. 10). Neglecting end effects, mean stress ($\bar{\sigma} = (\sigma_1 + \sigma_2 + \sigma_3)/3$) and fault normal stress both decrease as shear stress rises toward the failure condition, but increase again during the coseismic drop in shear stress (Sibson, 1991). Provided fluid pressure stays constant, frictional fault strength (dependent on normal stress) must also decrease during the interseismic period of increasing shear stress (load-weakening effect), only to increase again during coseismic relief of shear stress. In

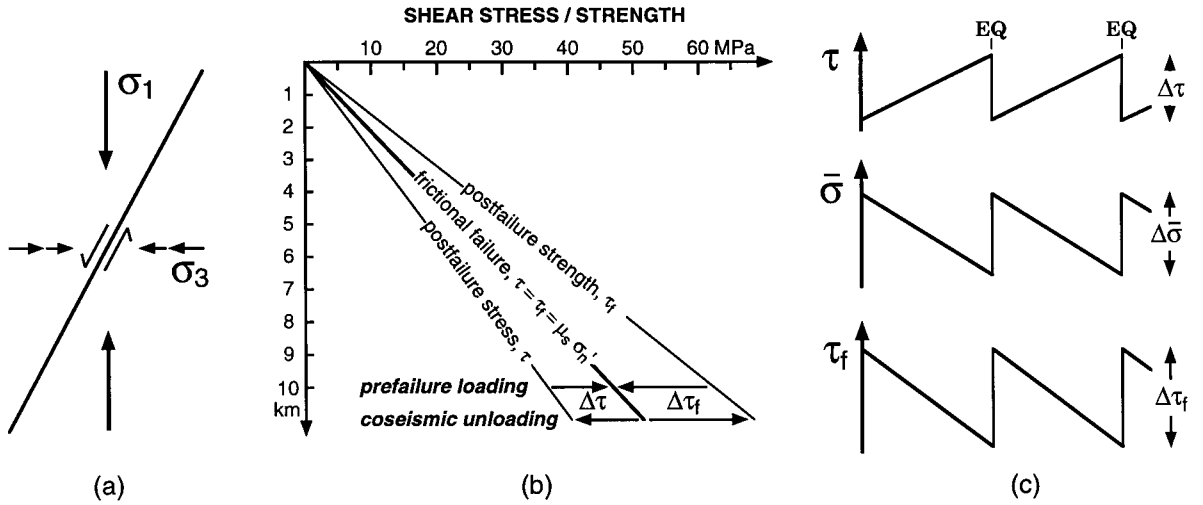

Fig. 10. Load-weakening character of an optimally oriented normal fault under hydrostatic fluid pressure (a) prefailure and postfailure stress state; (b) shear stress and strength at failure and postfailure after a coseismic shear stress drop, $\Delta\tau = 10$ MPa, at 10 km depth; (c) coupled cycling of mean stress, $\bar{\sigma}$ and frictional fault strength, τ_f, with shear stress on the fault (fluid pressure and σ_1 assumed constant throughout).

practice, fluid pressure is unlikely to stay constant throughout the earthquake stress cycle, especially during the coseismic–postseismic period of rapid shear stress release, and the coupling of mean stress to the shear stress cycling around a normal fault may lead to substantial fluid redistribution (see Section 5.2).

4.5. Comparative frictional strengths of non-optimally oriented normal faults

On the continuing assumption that $\sigma_v = \sigma_1$ Eq. (6) may be used to estimate the comparative frictional strengths of non-optimally oriented faults (all with poles in the σ_1/σ_3 plane) at a depth of 10 km for varying fault dips ($\delta = 90^\circ - \theta_r$), and for different values of the pore-fluid factor, λ_v (Fig. 11). For constant λ_v, the level of differential stress required for reactivation increases symmetrically as fault dip (and the reactivation angle) increase or decrease from the optimal orientation. Thus, as a set of planar normal faults 'dominos' to lower dips with ongoing crustal extension, the differential stress needed for further reactivation increases progressively if the fluid pressure level stays constant. The vertical dashed line at twice the optimal reactivation angle represents the angle of frictional lock-up for $\mu_s = 0.75$ (Sibson, 1985a). Shear reactivation of severely misoriented normal faults (the shaded area to the right of this line) is only possible when the tensile overpressure condition is met (i.e. $\sigma_3' < 0$ or $P_f > \sigma_3$).

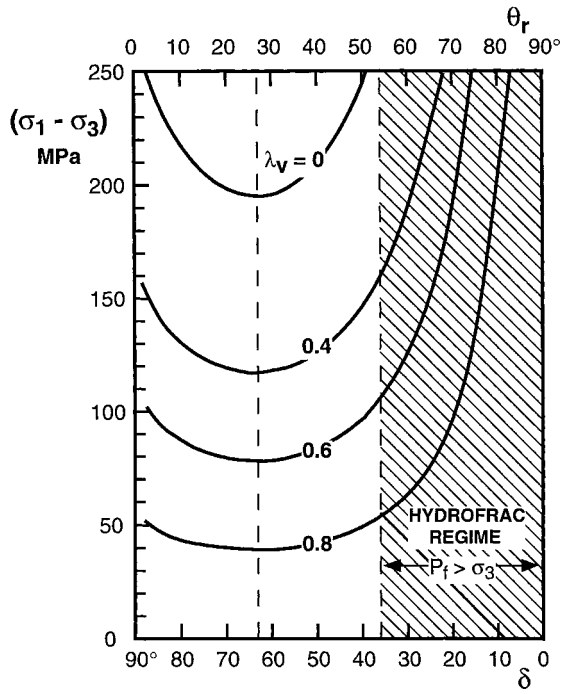

Fig. 11. Differential stress required for normal fault reactivation at 10 km depth with $\sigma_v = \sigma_1$ for varying dip angles, $\delta = 90^\circ - \theta_r$, and values of the pore-fluid factor, λ_v. Shading denotes severe misorientation where the tensile overpressure condition has to be met for reactivation ($\mu_s = 0.75$; $\rho = 2650$ kg/m^3).

The problem is that as the differential stress needed for reshear of the existing fault increase with decreasing fault dip, the stage may be reached where it becomes easier to form a new optimally oriented fault through failure of the surrounding intact crust rather than to continue reactivating the existing, unfavourably oriented structure. Profett (1977), for example, has described structural assemblages in Nevada where progressive crustal extension has involved successive generations of dominoing normal faults. This situation is illustrated on the brittle failure mode plot in Fig. 4 where the line representing the reshear criterion for a cohesionless fault dipping at 40° ($\theta_r = 50°$) intersects the failure curve for intact rock with $T = 5$ MPa at $\sigma'_v = 60$ MPa, corresponding to a depth of 4 km in a hydrostatically pressured regime. Thus for crust with $T = 5$ MPa, reactivation of an existing hydrostatically pressured fault with a dip of 40° would occur in preference to the formation of a new optimally oriented fault at depths less than 4 km, but at greater depths it would be easier to form a new normal fault than to reactivate the existing structure.

An existing fault is more likely to be reactivated in shear at non-optimal orientations if fluid overpressure is localised within the fault zone (see Hill, 1993). This is illustrated in Fig. 12, again derived from the reshear criterion (Eq. (6)). Here, the localised λ_v value needed for reshear of an overpressured nonoptimally oriented fault at the same level of differential stress as that required for reshear of an optimally oriented normal fault that is hydrostatically pressured ($\lambda_v = 0.4$) is plotted against fault dip. Only a moderate degree of localised overpressuring ($\lambda_v < 0.6$) is needed in a normal fault regime to keep the misoriented fault at comparable strength levels as dip values decrease down towards the angle of frictional lock-up.

Similar considerations may be applied to the incorporation of existing low-angle discontinuities (e.g. former thrust faults) within an active extensional fault system, the key

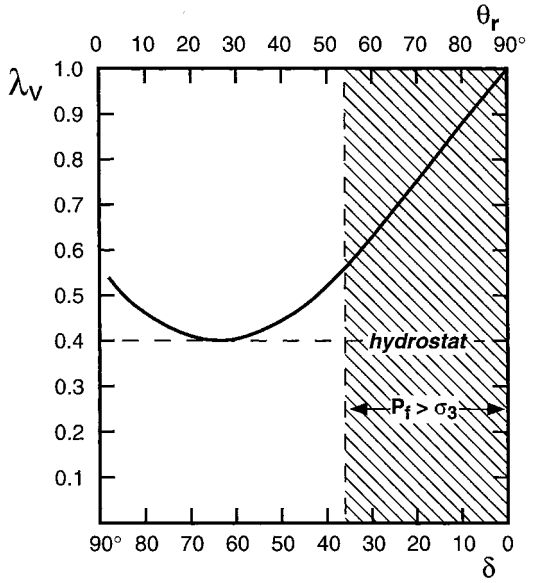

Fig. 12. Plot of localised λ_v needed for reshear of a misoriented fault ($\delta = 90° - \theta_r$) at the same level of differential stress as an optimally oriented normal fault under hydrostatic fluid pressure, $\lambda_v = 0.4$ ($\mu_s = 0.75$; $\rho = 2650$ kg/m^3).

requirement being that the more unfavourably oriented the existing structure, the greater the need for significant localised overpressuring within that structure. Note that while in principle the concepts developed here for 2D reactivation are readily extendable to 3D, in practice reactivation in 3D is critically dependent on the relative magnitude of the intermediate principal stress, σ_2, which is often ill constrained.

4.6. Containment of localised fluid overpressures

While the λ_v value needed for non-optimal reactivation of normal faults does not appear so extreme, what is really at issue is the value of σ_3' needed for reactivation because of its strong influence on rock permeability. Eq. (6) may be rewritten as

$$\sigma_3' = (\sigma_3 - P_f) = \frac{(1 - \mu_s \tan\theta_r)}{(1 + \mu_s \cot\theta_r)} \rho g z (1 - \lambda_v) \tag{8}$$

which allows the σ_3' value needed for reactivation to be plotted against reactivation angle (or dip) as a function of depth and λ_v. In Fig. 13, the value of σ_3' needed for frictional reshear at 10 km depth is plotted against dip for various values of the pore-fluid factor, λ_v. The essential point is that whatever the λ_v value, the σ_3' value must tend towards zero for continued reactivation as the lock-up angle ($\delta \sim 37^\circ$) is approached, requiring $P_f \rightarrow \sigma_3$. Because permeability generally increases at low effective stress (Seront et al., 1998; Morrow and Lockner, 1997), there is the potential for self-regulation of fluid overpressure, the likelihood of sustaining extreme fluid overpressure decreasing with diminishing σ_3'.

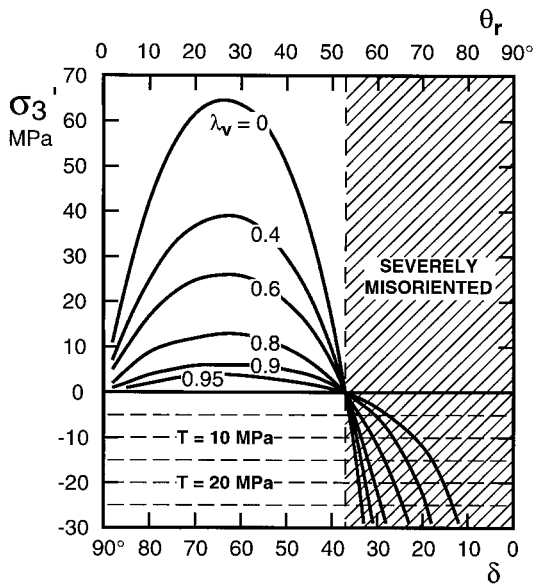

Fig. 13. Effective least compressive stress, σ_3', needed for frictional reshear at $z = 10$ km plotted against dip angle ($\delta = 90^\circ - \theta_r$) for various values of the pore-fluid factor, λ_v ($\mu_s = 0.75$; $\rho = 2650$ kg/m^3).

It is also apparent from Fig. 13 that normal fault reactivation with $\sigma_v = \sigma_1$ could potentially continue beyond the lock-up angle (that is, to still lower dips) provided the tensile overpressure condition, $\sigma_3' < 0$ (or $P_f > \sigma_3$), was maintained. In theory, frictional reactivation of cohesionless normal faults could occur under low differential stress levels down to extremely low dip angles if the fault wallrocks, especially on the hanging-wall, retain significant tensile strength (cf. Axen, 1992). For example, with $\delta = 10^\circ$, $\lambda_v = 0.99$, and $\sigma_3' = -10$ MPa at 10 km depth, frictional shear reactivation will occur with $(\sigma_1 - \sigma_3) \sim 10$ MPa. In practice, fluid loss through hydraulic extension or extensional-shear fracturing seems likely to limit the sustainability of the tensile overpressure condition. Observed dips of seismically active normal faults extending down to $\delta \sim 35^\circ$ (Fig. 8(a)) are generally consistent with expected frictional

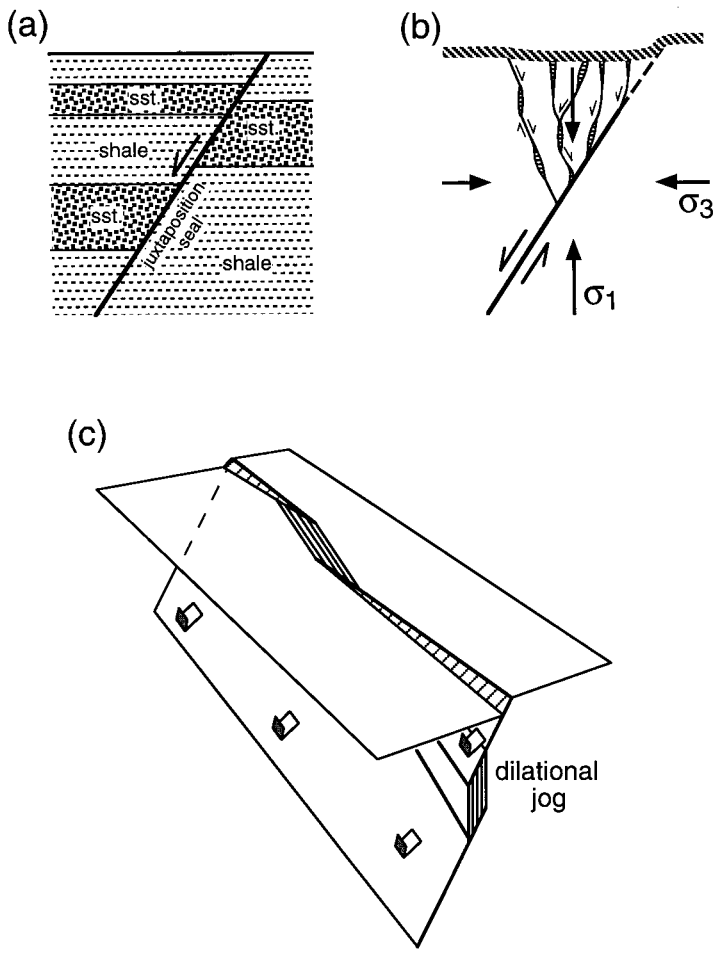

Fig. 14. Passive fluid interactions with normal faults: (a) stratal juxtaposition (permeable sandstone against impermeable shale) forming a sealing barrier; (b) high-permeability horsetail mesh developed near-surface in hanging wall of a normal fault; (c) gently raking dilation jog within normal fault zone, showing surface expression.

'lock-up' for vertical σ_1 and 'Byerlee' coefficients of rock friction with $P_f \rightarrow \sigma_3$, but not for $P_f > \sigma_3$.

5. Fluid interactions with normal fault systems

It is apparent that a diverese range of interactions may occur between aqueous pore fluids and normal faults depending, among other factors, on depth in the crust, the host rocks to the fault system, the level of fault activity, and the general tectonic framework. Fluid interactions may be broadly grouped into those that are essentially static, where the fault system behaves either as a passive barrier to flow or as a fluid conduit, and those that are inherently dynamic with episodes of fluid redistribution modulated by fault slip increments coupled to the seismic stress cycle. The following discussion reviews some of the interactions that have to be considered in different settings.

5.1. Static interactions

Interactions between passive normal faults and fluid flow depend critically on the relative permeability between the fault zone and the host rocks (cf. Section 2.5). At high crustal levels, inactive faults in sedimentary basins often act as relatively impermeable sealing barriers to both cross-fault and along-fault migration through various combinations of localised cataclastic grainsize reduction in initially high porosity sands, the presence of clay 'smears' along the faults, hydrothermal alteration and cementation of fault gouge, and from the juxtaposition of impermeable against permeable strata (Fig. 14(a)) (Knott, 1993; Knipe, 1997). There are indications that the probability of a strong fault seal increases with finite displacement.

By contrast, for normal fault systems developed in competent low-porosity rocks (volcanic, plutonic, metamorphic), a high degree of subsidiary brittle deformation may develop in the near-surface in the form of 'horse-tailing' extensional fault-fracture meshes developed in the fault hanging wall, especially if the principal fault retains cohesive strength through hydrothermal cementation (Fig. 14(b)). These serve as permeable conduits focusing topographically driven flow and/or magmatically induced hydrothermal convection. The depth extent over which these high-permeability flow systems may extend is a function of rock tensile strength and is affected by processes such as silicification of the rock-mass (cf. Sections 2.3 and 2.4). Fault-fracture meshes of high relative permeability may also develop at greater depths in sites such as dilational fault jogs where σ_3 has been locally reduced (Segall and Pollard, 1980).

Strong σ_2 directional permeability parallel to strike may develop in such settings, locally deflecting buoyancy-driven convective flow. The vigorous hydrothermal circulation associated with mid-ocean spreading ridges clearly utilises such extensional fault-fracture systems and, at least locally, includes components of along-strike flow (Haymon et al., 1991; Fisher, 1998). Curewitz and Karson (1997) note the preferential location of active hot springs at fault terminations, intersections, and overlap areas such as relay ramps, suggesting that these active process zones associated with fault growth retain the highest fracture permeabilities. It seems possible, however, that at least some of these fault overlap areas may represent the surface

projection of high permeability dilational jogs that rake gently in the principal slip surfaces (Fig. 14(c)) (see discussion of Comstock Lode in Section 5.2.2).

5.2. Dynamic interactions

Two complexly interlinked factors, episodic changes in the tectonic stress state and fault zone permeability may modulate fluid flow around seismically active normal faults. Through the load-weakening character of normal faults, the horizontal least compressive stress, $\sigma_h = \sigma_3$, the mean stress and fault normal stress all decrease during progressive loading, only to increase again at failure, while the vertical stress, $\sigma_v = \sigma_1$, stays constant (Figs. 10 and 15(a); see

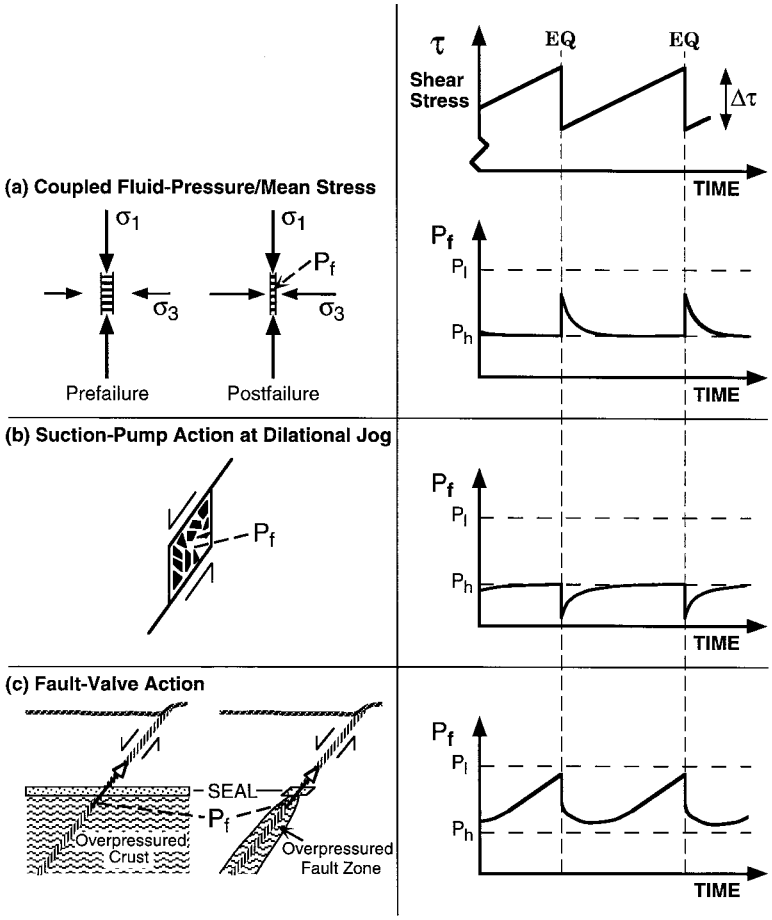

Fig. 15. Dynamic fluid interactions coupled to the seismic shear stress cycle on normal faults (EQ: seismic slip increment, P_h: hydrostatic fluid pressure, P_l: lithostatic fluid pressure): (a) fluid pressure rise from fracture closure linked to increased horizontal and mean stress at failure; (b) localised coseismic reduction of fluid pressure within a dilational fault jog; (c) fault-valve action from both distributed and localised overpressuring beneath sealing horizons.

Section 4.4). Fault zone permeability is likely to be the highest in the post-seismic period immediately following rupture (Brown and Bruhn, 1996) but may also vary throughout the loading cycle. Processes such as solution transfer in fine-grained gouge and hydrothermal cementation act to reduce permeability through the interseismic period, though this may be counteracted by the progressive decrease in fault normal stress. High permeability on normal faults postfailure may also be counteracted to some extent by increased fault normal stress. At least three dynamic processes, acting singly or in combination, may contribute to fluid redistribution around normal faults.

5.2.1. Mean stress cycling

Changes in the horizontal least stress, $\sigma_h = \sigma_3$ and the mean stress, $\bar{\sigma}$ tied to the accumulation and release of shear stress on normal faults (Fig. 10), may cause substantial fluid redistribution, especially in near-surface, high porosity rocks. In terms of bulk effects, progressive of reduction of σ_3 and $\bar{\sigma}$ through the interseismic period should lead to positive dilation of porosity and vertical fractures and the drawing-in of fluid. The sudden increase in σ_3 and $\bar{\sigma}$ accompanying normal fault rupture leads to a transitory increase in fluid pressure and expulsion of contained fluid (Fig. 15(a)), likely accounting for the major distributed surface effusions that have sometimes been observed following normal slip earthquakes (Sibson, 1991; Muir-Wood and King, 1993). Stress heterogeneities at rupture tips and overlaps may locally complicate the pattern of fluid redistribution.

5.2.2. Suction pump effects at dilational irregularities

Rapid coseismic dilation induced at specific structural sites such as dilational fault jogs and bends may induce localised transient reductions in fluid pressure (Fig. 15), leading to brecciation of surrounding wallrock by hydraulic implosion from the fluid pressure imbalance and focused postseismic inflow (Sibson, 1985b, 1986). Fault-fracture meshes formed in such dilational sites are especially common in the hanging walls of normal faults in the near-surface but also arise at depth in areas of stress heterogeneity or fluid overpressure where the tensile overpressure condition, $\sigma_3' < 0$, is met. Architecture of dilational jogs is critical to 3D fluid redistribution (Fig. 14(c)). For instance, the distribution of bonanza lodes over 5 km strike distance in the plane of the Ag–Au Comstock Lode, Nevada (Vikre, 1989), is strongly suggestive of a gently raking dilational jog in the hosting normal fault.

5.2.3. Fault-valve action

Postseismic valving discharge as a consequence of enhanced permeability postfailure may occur either where normal faults transect seals capping broad regions of suprahydrostatically pressured crust, or where the normal fault zone at depth is itself locally overpressured with respect to its surroundings (Fig. 15(c)). Though doubts are often expressed about the sustainability of fluid overpressures in extending crust, there is good evidence for overpressures approaching lithostatic beneath shale sequence or hydrothermal sealing caps in many extensional basins (Hunt, 1990). Moreover, diagnetic assemblages adjacent to normal faults (Burley et al., 1989) and the presence of localised thermal plumes in the high levels of some basins (Roberts et al., 1996; McKenna and Sharp, 1997), provide evidence that normal faults

can indeed function as 'valves' that intermittently discharge fluid from overpressured portions of the basins.

Fluid inclusion evidence from the crystalline footwalls of major active normal faults in the Basin and Range coupled to structural evidence in the form of sets of steep extension veins and conjugate extensional-shears (which also occur in core complex assemblages) suggest that fluid overpressuring does also occur in crystalline rocks, but is localised within the normal fault zones which function as fluid conduits from the mid-crust (Parry and Bruhn, 1990; Bruhn et al., 1994; Reynolds and Lister, 1987; Axen and Selverstone, 1994). The inclusions also provide evidence for fluid-pressure cycling from near-lithostatic to hydrostatic values at depths corresponding roughly with the base of the seismogenic zone.

By analogy with steep reverse faults where valve action reaches its most extreme form when the faults are severely misoriented (i.e. oriented at beyond the lock-up angle), the most intense valve action in extensional regimes would be expected to occur in association with low-dipping normal faults ($\delta < 35^\circ$) that are severely misoriented at high angles to vertical σ_1. However, fault-valve action in extensional regimes is unlikely to involve such large fluid volumes or such intense fluid pressure cycling as in compressional regimes because increased fault normal stress postfailure and vertical fracture orientation limit the degree of overpressuring and the quantity of overpressured fluid that can readily gain access to the fault for postfailure discharge (Sibson and Scott, 1998). Note, however, that valving discharge of quite small fluid volumes in low-porosity rocks can still induce significant increases in fault strength affecting the recurrence and the initiation of the next normal fault rupture (Sibson, 1992).

5.3. Hydraulic communication along strike

The strong subhorizontal σ_2 permeability expected in normal fault systems raises the possibility of along-strike hydraulic communication. This is of interest given the tendency for earthquake sequence in extensional fault systems, to involve multiple ruptures and aftershock

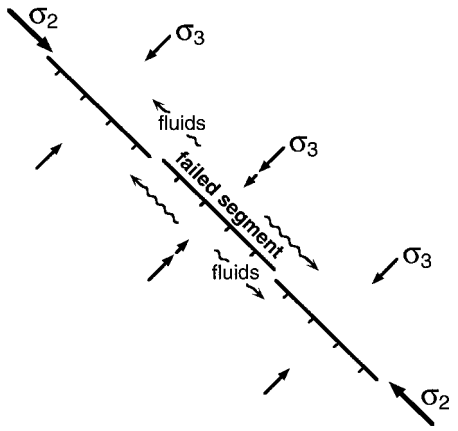

Fig. 16. Cartoon of a segmented normal fault system illustrating fluid transfer in the σ_2 direction along strike from a ruptured segment as a consequence of postfailure increase in the levels of least stress, σ_3, and mean stress, $\bar{\sigma}$.

activity migrating along strike. Examples include the 1954 coupled $M \sim 7$ normal fault ruptures at Fairview Peak and Dixie Valley, Nevada, separated by only 4 min (Hodgkinson et al., 1996; Caskey and Wesnousky, 1997), the 1989 Dobi graben sequence in Central Afar with ten $M > 5.5$ earthquake epicentres migrating along a strike distance of 50 km in ~50 h (Noir et al., 1997), and the 1997–98 Umbria-Marche sequence in the central Appennines with six $M > 5$ earthquakes and a rich aftershock sequence progressively extending along strike (Amato et al., 1998).

While Coulomb modelling of static stress interaction does much to explain coupled failure between adjacent normal fault segments (e.g. Hodgkinson et al., 1996; Nostro et al., 1997), the large range of observed interaction times (from seconds to months) suggests some form of viscous component to the interaction that could arise from the propagation of a fluid pressure wave through a fractured rock-mass, as Noir et al. (1997) have suggested for the Afar sequence. An argument can be made that the boosted fluid pressure resulting from increased horizontal σ_3 and mean stress consequent on failure of one normal fault segment, coupled to σ_2 directional permeability, causes fluid to migrate along strike from the initial rupture, thereby triggering further rupturing through reduction of effective fault-normal stress (Fig. 16). But at what depth would such migration occur? The hydrostatically pressured, high-permeability zone of near-surface subsidiary fracturing must be dominated by topographically driven flow and seems unlikely to influence rupture nucleation at depth. High strike-parallel permeability could also be maintained, however, in deeper, overpressured portions of normal fault zones beneath sealing levels. The tantalising evidence for fluid overpressuring towards the base of the seismogenic zone suggests that hydraulic communication along strike could be important in this critical region where larger ruptures tend to nucleate.

5.4. Hydrothermal mineralisation in normal fault systems

The principal site for precious metal mineralisation in normal fault systems is the epizonal near-surface environment where high-permeability fault-fracture meshes allowing large fluid flux coincide with the boiling horizon for ascending hydrothermal plumes and also allow mixing of fluids from different sources (Henley, 1985; Vikre, 1989). Depth of open fracturing (Section 2.3), affecting the vertical range over which mineralization may occur, depends on rock tensile strength which may increase as silicification pervades the rock-mass. Permeability within such mesh structures may be intermittently renewed by earthquake rupturing. Similar structural considerations affect the development of SEDEX (sedimentary exhalative) deposits, some of which apparently result from single-pass dewatering of major sedimentary basins along marginal growth normal (and/or strike-slip) faults, perhaps aided by coeval magmatism (Goodfellow et al., 1993; Johnston et al., 1996). In essence, this represents a form of sustained but probably episodic discharge from the depths of an overpressured basin with the normal faults functioning as valves. Spencer and Welty (1986) also suggest that Cu–Pb–Zn–Ag–Au mineralization developed in the highly fractured top 1–3 km of detachment fault systems results from the mixing, with cold high-level oxidised fluids, of hot reduced, metal-bearing fluids ascending along the shallow dipping detachment faults and deriving heat from the rising lower plate.

Deeper mesozonal lode gold mineralization is only rarely hosted by normal faults (for

example in the Mesozoic Otago Schist belt of southern New Zealand) and the mineralisation is generally less intense than in compressional regimes (Sibson and Scott, 1998). However, major Au–quartz mineralisation in the Alaska–Juneau Mine, SE Alaska, occupies an extensional fault-fracture mesh developed at >5 km depth (Miller et al., 1992), apparently self-generated by overpressured fluids during a transitory (and probably localised) switch from a compressional to an extensional stress regime which decreased the level of fluid overpressure that could be sustained.

6. Discussion

A range of field evidence from exhumed normal fault zones suggests that aqueous fluids are intimately involved with normal faulting throughout and below the seismogenic regime, playing a key role in frictional fault mechanics through the principle of effective stress. The level of fluid pressure in relation to vertical stress dictates the style of extensional structures that may develop and, alongwith other mechanical considerations, affects the development of fault-hosted mineralization.

For (Byerlee's, 1978) range of rock friction coefficients, the dip-angle for frictional lock-up of normal faults under vertical σ_1 is $35 \pm 5^\circ$. The observed dip range for normal fault ruptures ($65^\circ > \delta > 35^\circ$) is not only consistent with this expected frictional 'lock-up' for dominoing normal faults, but also suggest that reactivation frequently occurs with the overpressure condition, $P_f \rightarrow \sigma_3$, localised in the fault zones to inhibit the formation of new, more favourably oriented normal faults. Because the hydrofracture condition in the vicinity of cohesionless normal faults is unattainable if fault dip remains greater than the frictional lock-up dip, overpressures will generally be regulated by fault-valve action rather than by hydraulic extension fracturing. Normal fault reactivation at lower dips under vertical σ_1 is theoretically possible if the tensile overpressure condition, $P_f > \sigma_3$, can be maintained by high tensile strength of the fault hanging wall, but lack of observed rupture dips below 35° suggests this is a rare circumstance.

Prevalence of subhorizontal σ_2 directional permeability around normal faults raises the interesting possibility of hydraulic communication along strike, which would do much to explain observed along-strike migration of seismic activity in normal fault systems. The 3D geometry of structural components within such systems is thus clearly of enormous importance in establishing the degree of fluid coupling.

Proper understanding of normal fault mechanics still requires full answers to critical questions such as the extent to which stress trajectories become curved at depth in extensional regimes, and the factors that allow localised overpressuring of crustal-scale normal fault zones at depth.

Acknowledgements

I thank Professor Giuseppe Cello and the organisers of the International Workshop 'The Resolution of Geological Analysis and Models for Earthquake Faulting Studies' for the

opportunity to participate in the Camerino workshop. Research leading to this paper was funded from the NZ Public Good Science Fund through FRST Contract #CO5611.

References

Amato, A., Azzara, R., Chiarabba, C., Cimini, G.B., Cocco, M., Di Bona, M., Margheriti, L., Mazza, S., Mele, F., Selvaggi, G., Basili, A., Boschi, E., Courboulex, F., Deschamps, A., Gaffet, S., Bittarelli, G., Chiaraluce, L., Piccinini, D., Ripepe, M., 1998. The 1997 Umbria-Marche, Italy, earthquake sequence: a first look at the main-shocks and aftershocks. Geophysical Research Letters 25, 2861–2864.

Anderson, E.M., 1905. The dynamics of faulting. Transactions Edinburgh Geological Society 8, 387–402.

Antonellini, M., Aydin, A., 1994. Effect of faulting on fluid flow in porous sandstones: petrophysical properties. American Association of Petroleum Geologists Bulletin 78, 355–377.

Axen, G.J., 1992. Pore pressure, stress increase, and fault weakening in low-angle normal faulting. Journal of Geophysical Research 97, 8979–8991.

Axen, G.J., Selverstone, J., 1994. Stress state and fluid pressure level along the Whipple detachment fault, California. Geology 22, 835–838.

Bally, A.W., Bernouilli, D., Davis, G.A., Montadert, L., 1980. Listric normal faults. In: Oceana Acta, Proceedings 26th International Geological Congress, Paris, 87–101.

Barton, C., Zoback, M.D., Moos, D., 1995. Fluid flow along potentially active faults in crystalline rock. Geology 23, 683–686.

Brace, W.F., 1984. Permeability of crystalline rocks: new in situ measurements. Journal of Geophysical Research 89, 4327–4330.

Bradshaw, G.A., Zoback, M.D., 1988. Listric normal faulting, stress refraction, and the state of stress in the Gulf Coast basin. Geology 16, 271–274.

Brown, S.R., Bruhn, R.L., 1996. Formation of voids and veins during faulting. Journal of Structural Geology 18, 657–671.

Bruhn, R.L., Parry, W.L., Yonkee, W.A., Thompson, T., 1994. Fracturing and hydrothermal alteration in normal fault zones. Pure and Applied Geophysics 142, 609–644.

Burley, S.D., Mullis, J., Matter, A., 1989. Timing diagenesis in the Tartan reservoir (UK North Sea): constraints from combined cathodoluminescence spectroscopy and fluid inclusion studies. Marine and Petroleum Geology 6, 98–120.

Byerlee, J.D., 1978. Friction of rocks. Pure and Applied Geophysics 116, 615–626.

Caine, J.S., Evans, J.P., Forster, C.B., 1996. Fault zone architecture and permeability structure. Geology 24, 1025–1028.

Caskey, S.J., Wesnousky, S.G., 1997. Static stress changes and earthquake triggering during the 1954 Fairview Peak and Dixie Valley earthquakes, central Nevada. Bulletin of the Seismological Society of America 87, 521–527.

Cowie, P.A., 1998. A healing-reloading feedback control on the growth rate of seismogenic normal faults. Journal of Structural Geology 20, 1075–1087.

Curewitz, D., Karson, J.A., 1997. Structural settings of hydrothermal outflow: fracture permeability maintained by fault propagation and interaction. Journal of Volcanology and Geothermal Research 79, 149–168.

Davis, G.H., 1983. Shear zone model for the origin of metamorphic core complexes. Geology 11, 342–347.

Evans, J., 1990. Textures, deformation mechanisms, and the role of fluids in the cataclastic deformation of granitic rocks. In: Knipe, R.J., Rutter, E.H. (Eds.), Deformation Mechanisms, Rheology, and Tectonics, vol. 54. Geological Society, London, pp. 29–39 (Special Publication).

Evans, J.P., Forster, C.B., Goddard, J.V., 1997. Permeability of fault-related rocks, and implications for hydraulic structure of fault zones. Journal of Structural Geology 19, 1393–1404.

Fisher, A.T., 1998. Permeability within basaltic oceanic crust. Reviews of Geophysics 36, 143–182.

Goodfellow, W.D., Lydon, J.W., Turner, R.J.W., 1993. Geology and genesis of stratiform sediment hosted (SEDEX) zinc–lead–silver sulphide deposits. In: Kirkham, R.V., Sinclair, W.D., Thorpe, R.I., Duke, J.M. (Eds.), Mineral Deposit Modeling, vol. 40. Geological Association of Canada, Canada, pp. 201–251 (Special Paper).

Groshong, R.H., 1988. Low-temperature deformation mechanisms and their interpretation. Geological Society of America Bulletin 100, 1329–1360.

Hardman, R.F.P., Booth, J.E., 1991. The significance of normal faults in the exploration and production of hydrocarbons. In: Roberts, A.M., Yielding, G., Freeman, B. (Eds.), The Geometry of Normal Faults, vol. 56. Geological Society, London, pp. 1–13 (Special Publication).

Haymon, R.M., Fornari, D.J., Edwards, M.H., Carbotte, S., Wright, D., MacDonald, K., 1991. Hydrothermal vent distribution along the East Pacific Rise crest (9°09′–54′N) and its relationship to magmatic and tectonic processes on fast-spreading mid-ocean ridges. Earth and Planetary Science Letters 104, 513–534.

Henley, R.W. 1985. The geothermal framework for epithermal deposits. In: Berger, B.R., Bethke, P.M. (Eds.), Geology and Geochemistry of Epithermal Systems, Reviews of Economic Geology, vol. 2, pp. 1–24.

Hickman, S.H., Barton, C.A., Zoback, M.D., Morin, R., Sass, J., Benoit, R., 1997. In-situ stress and fracture permeability along the Stillwater fault zone, Dixie Valley, Nevada. International Journal of Rock Mechanics and Mining Science 34, 1–10.

Hill, D.P., 1977. A model for earthquake swarms. Journal of Geophysical Research 82, 1347–1357.

Hill, D.P., 1993. A note on ambient pore pressure, fault-confined pore pressure, and apparent friction. Bulletin of the Seismological Society of America 83, 583–586.

Hodgkinson, K.M., Stein, R.S., King, G.C.P., 1996. The 1954 Rainbow Mountain, Dixie Valley, Fairview Peak earthquakes: a triggered normal faulting sequence. Journal of Geophysical Research 101, 25459–25471.

Hubbert, M.K., Rubey, W.W., 1959. Role of fluid pressure in mechanics of overthrust faulting. Geological Society of America Bulletin 70, 115–166.

Hunt, J.M., 1990. Generation and migration of petroleum from abnormally pressured fluid compartments. American Association of Petroleum Geologists Bulletin 74, 1–12.

Jackson, J.A., White, N.J., 1989. Normal faulting in the upper continental crust: observations from regions of active extension. Journal of Structural Geology 11, 15–36.

Jackson, J.A., Blenkinsop, T., 1997. The Bilila–Mtakataka fault in Malawi: an active 100 km long normal fault segment in thick seismogenic crust. Tectonics 16, 137–150.

Jaeger, J.C., Cook, N.G.W., 1979. Fundamentals of Rock Mechanics. Methuen, London.

John, B.E., Foster, D.A., 1993. Structural and thermal constraints on the initiation angle of detachment faulting in the southern Basin and Range: the Chemehuevi Mountains case study. Geological Society of America Bulletin 105, 1091–1108.

Johnston, J.D., Coller, D., Millar, G., Critchley, M.F., 1996. Basement structural controls on Carboniferous-hosted base metal mineral deposits in Ireland. In: Strogen, P., Somerville, I.D., Jones, G.L. (Eds.), Recent Advances in Lower Carboniferous Geology, vol. 107. Geological Society, London, pp. 1–21 (Special Publication).

Kerrich, R., 1988. Detachment zones of Cordilleran metamorphic core complexes. Geologische Rundschau 77, 157–182.

Knipe, R.J., 1997. Juxtaposition and seal diagrams to help analyze fault seals in hydrocarbon reservoirs. American Association of Geologists Bulletin 81, 187–195.

Knott, S.D., 1993. Fault seal analysis in the North Sea. American Association of Petroleum Geologists Bulletin 77, 778–792.

Lister, G.S., Davis, G.A., 1989. The origin of metamorphic core complexes and detachment faults formed during Tertiary continental extension in the northern Colorado River region, USA. Journal of Structural Geology 11, 65–93.

Lockner, D.A. 1995. Rock failure. In: Ahrens, T.J. (Eds.), Rock Physics and Phase Relations: A Handbook of Physical Constants, American Geophysical Union Reference Shelf, Washington, vol. 3, pp. 127–147.

McClay, K., Khalil, S., 1998. Extensional hard linkages, Gulf of Suez. Geology 26, 563–566.

McKenna, T.E., Sharp, J.M., 1997. Subsurface temperatures, fluid pressures, and salinities in the Rio Grande embayment, Gulf of Mexico basin, USA. In: Proceedings 30th International Geological Congress, vol. 8, 263–274.

Machette, M.N., Personius, S.F., Nelson, A.R., Schwartz, D.P., Lund, W.R., 1991. The Wasatch fault zone, Utah — segmentation and history of earthquakes. Journal of Structural Geology 13, 137–149.

Melosh, J., 1990. Mechanical basis for low-angle normal faulting in the Basin and Range province. Nature 343, 331–335.

Miller, L.D., Barton, C.C., Fredericksen, R.S., Bressler, J.R., 1992. Structural evolution of the Alaska–Juneau gold deposit, Southeastern Alaska. Canadian Journal of Earth Science 29, 865–878.

Moore, D.E., Lockner, D.A., Byerlee, J.D., 1994. Reduction of permeability in granite at elevated temperatures. Science 265, 1558–1561.

Morrow, C.A., Lockner, D.A., 1997. Permeability and porosity of the Illinois UPH 3 drillhole granite and a comparison with other deep drillhole rocks. Journal of Geophysical Research 102, 3067–3075.

Muir-Wood, R., King, G.C.P., 1993. Hydrological signatures of earthquake strain. Journal of Geophysical Research 98, 22035–22068.

Noir, J., Jacques, E., Bekri, S., Adler, P.M., Tapponier, P., King, G.C.P., 1997. Fluid flow triggered migration of events in the 1989 Dobi earthquake sequence of Central Afar. Geophysical Research Letters 24, 2335–2338.

Nostro, C., Cocco, M., Belardinelli, M.E., 1997. Static stress changes in extensional regimes: an application to Southern Apennines, Italy. Bulletin of the Seismological Society of America 87, 234–248.

Parry, W.T., Bruhn, R.L., 1986. Pore fluid and seismogenic characteristics of fault rock at depth on the Wasatch Fault, Utah. Journal of Geophysical Research 91, 730–744.

Parry, W.T., Bruhn, R.L., 1987. Fluid inclusion evidence for minimum 11 km vertical offset on the Wasatch Fault, Utah. Geology 22, 67–70.

Parry, W.T., Bruhn, R.L., 1990. Fluid pressure transients on seismogenic normal faults. Tectonophysics 179, 335–344.

Parsons, T., Thompson, G.A., 1993. Does magmatism influence low-angle normal faulting? . Geology 21, 247–250.

Paterson, M.S., Luan, F.C., 1990. Quartzite rheology under geological conditions. In: Knipe, R.J., Rutter, E.H. (Eds.), Deformation Mechanisms, Rheology, and Tectonics, vol. 54. Geological Society, London, pp. 299–307 (Special Publication).

Peacock, D.C.P., Sanderson, D.J., 1991. Displacements, segment linkage, and relay ramps in normal fault zones. Journal of Structural Geology 13, 721–733.

Power, W.L., Tullis, T.E., 1989. The relation between slickenside surfaces in fine-grained quartz and the seismic cycle. Journal of Structural Geology 11, 879–893.

Profett, J.M., 1977. Cenozoic geology of the Yerington district, Nevada, and implications for the nature of Basin and Range faulting. Geological Society of America Bulletin 88, 247–266.

Reynolds, S.J., Lister, G.S., 1987. Structural aspects of fluid-rock interactions in detachment zones. Geology 15, 362–366.

Roberts, S.J., Nunn, J.A., Cathles, L., Cipriani, F.-D., 1996. Expulsion of abnormally pressured fluids along faults. Journal of Geophysical Research 101, 28231–28252.

Rutter, E.H., Brodie, K.H., 1992. Rheology of the lower crust. In: Fountain, D.M., Arculus, R., Kay, R.W. (Eds.), Continental Lower Crust, Developments in Geotectonics, vol. 23. Elsevier, Amsterdam, pp. 201–267.

Schlische, R.W., Young, S.S., Ackermann, R.V., Gupta, A., 1996. Geometry and scaling relations of a population of very small rift-related normal faults. Geology 24, 683–686.

Scholz, C.H., Dawers, N.H., Yu, J.-Z., Anders, M.H., Cowie, P.A., 1993. Fault growth and fault scaling laws: preliminary results. Journal of Geophysical Research 98, 21951–21961.

Secor, D.T., 1965. Role of fluid pressure in jointing. American Journal of Science 263, 633–646.

Segall, P., Pollard, D.D., 1980. Mechanics of discontinuous faults. Journal of Geophysical Research 85, 4337–4350.

Seront, B., Wong, T.-F., Caine, J.S., Forster, C.B., Bruhn, R.L., Fredrich, J.T., 1998. Laboratory characterization of hydromechanical properties of a seismogenic normal fault system. Journal of Structural Geology 20, 865–882.

Sibson, R.H., 1983. Continental fault structure and the shallow earthquake source. Journal of the Geological Society, London 140, 741–767.

Sibson, R.H., 1985a. A note on fault reactivation. Journal of Structural Geology 27, 751–754.

Sibson, R.H., 1985b. Stopping of earthquake ruptures at dilational fault jogs. Nature 316, 248–251.

Sibson, R.H., 1986. Brecciation processes in fault zones: inferences from earthquake rupturing. Pure and Applied Geophysics 124, 159–175.

Sibson, R.H., 1991. Loading of faults to failure. Bulletin of the Seismological Society of America 81, 2493–2497.

Sibson, R.H., 1992. Implications of fault-valve behavior for rupture nucleation and recurrence. Tectonophysics 18, 1031–1042.

Sibson, R.H., 1994. Crustal stress, faulting, and fluid flow. In: Parnell, J. (Ed.), Geofluids: Origin, Migration and Evolution of Fluids in Sedimentary Basins, vol. 78. Geological Society, London, pp. 69–84 (Special Publication).

Sibson, R.H., 1996. Structural permeability of fluid-driven fault-fracture meshes. Journal of Structural Geology 18, 1031–1042.

Sibson, R.H., 1998. Brittle failure mode plots for compressional and extensional tectonic regimes. Journal of Structural Geology 20, 655–660.

Sibson, R.H., Scott, J., 1998. Stress/fault controls on the containment and release of overpressured fluids: examples from gold–quartz vein systems in Juneau, Alaska, Victoria, Australia, and Otago, New Zealand. Ore Geology Reviews 13, 293–306.

Sillitoe, R.H., 1993. Epithermal models: genetic types, geometrical controls and shallow features. In: Kirkham, R.V., Sinclair, W.D., Thorpe, R.I., Duke, J.M (Eds.), Mineral Deposit Modeling, vol. 40. Geological Association of Canada, Canada, pp. 403–417 (Special Paper).

Spencer, J.E., Welty, J.W., 1986. Possible controls of base-and precious-metal mineralization associated with lower Tertiary detachment faults in the lower Colorado River trough, Arizona and California. Geology 14, 195–198.

Stewart, I.S., Hancock, P.L., 1991. Scales of structural heterogeneity within neotectonic normal fault zones in the Aegean region. Journal of Structural Geology 13, 191–204.

Vendeville, B., 1991. Mechanisms generating normal fault curvature: a review illustrated by physical models. In: Roberts, A.M., Yielding, G., Freeman, B. (Eds.), The Geometry of Normal Faults, vol. 56. Geological Society, London, pp. 241–249 (Special Publication).

Vikre, P.G., 1989. Fluid-mineral relations in the Comstock Lode. Economic Geology 84, 1574–1613.

Walsh, J.J., Watterson, J., 1991. Geometric and kinematic coherence and scale effects on normal fault systems. In: Roberts, A.M., Yielding, G., Freeman, B. (Eds.), The Geometry of Normal Faults, vol. 56. Geological Society, London, pp. 193–203 (Special Publication).

Wells, D.L., Coppersmith, K.J., 1994. New empirical relationships among magnitude, rupture length, rupture width, rupture area, and surface displacement. Bulletin of the Seismological Society of America 84, 974–1002.

Westaway, R., 1991. Continental extension on sets of parallel faults: observational evidence and theoretical models. In: Roberts, A.M., Yielding, G., Freeman, B. (Eds.), The Geometry of Normal Faults, vol. 56. Geological Society, London, pp. 143–169 (Special Publication).

Westaway, R., 1998. Dependence of active normal fault dips on lower crustal flow regimes. Journal of the Geological Society, London 155, 233–254.

Wills, S., Buck, W.R., 1997. Stress-field rotation and rooted detachment faults: a Coulomb failure analysis. Journal of Geophysical Research 102, 20503–20514.